Adsorption Behaviors of HiPco Single-Walled Carbon Nanotube Aggregates for Alcohol Vapors

Cheol-Min Yang,[†] Hirofumi Kanoh,[‡] Katsumi Kaneko,*[,‡,§] Masako Yudasaka,[†] and Sumio Iijima[†,||]

Japan Science and Technology Corporation, NEC Corporation, 34 Miyukigaoka, Tsukuba 305-8501, Japan, Department of Physics, Meijo University, 1-501 Shiogamaguchi, Tempaku, Nagoya 468-8502, Japan, Department of Chemistry, Faculty of Science, Chiba University, 1-33 Yayoi, Inage, Chiba 263-8522, Japan, and Center for Frontier Electronics and Photonics, Chiba University, 1-33 Yayoi, Inage, Chiba 263-8522, Japan

Received: March 15, 2002; In Final Form: July 8, 2002

HiPco single-walled carbon nanotubes (HPNTs) containing Fe were purified by a one-step process with HCl-washing (D-method) and a two-step process with HCl-washing after air oxidation (GD-method). The HPNT samples before and after purification were characterized using the N_2 adsorption at 77 K, thermogravimetric analysis (TGA), and X-ray photoelectron spectroscopy (XPS). The TGA results showed a decreased Fe content after purification. In addition, the XPS results provided evidence that oxygen-based functional groups were introduced to the nanotube surface by both purification methods. The purification treatments also altered the N_2 adsorption isotherms from type II to type IV; this accompanied the development of microporosity. Thus, purification considerably affects the surface chemistry and pore structures of HPNT aggregates. The effects of purification on the adsorption properties of HPNT aggregates with regard to CH_3OH and C_2H_5OH vapors were examined at 303 K. The purification greatly enhanced the adsorptivity for CH_3OH and C_2H_5OH vapors at 303 K under a low relative pressure. We associated this with the enhanced microporosity and the oxygen-based functional groups introduced on the surface.

Introduction

Carbon nanotubes,[1,2] which have a tubular morphology with a tube diameter of several nanometers, have great potential for nanotechnological application in various fields such as gas storage,[3−5] field emission displays,[6] and supercapacitors.[7,8] In particular, the reversible storage of hydrogen on carbon nanotubes has attracted much attention from the energy and environmental protection fields.[3−5] As a new type of nanoporous carbon, carbon nanotubes have also been studied for use as adsorbents for gas adsorption.[9]

The relationship between surface functional groups and the adsorption properties of porous carbons has been actively studied.[10−13] Yang et al.[14,15] reported the adsorption behaviors of nitrogen- and iodine-doped activated carbon fibers (ACFs) for polar molecules and NO at 303 K. Single-walled carbon nanotubes (SWNTs) prepared by a catalytic method contain impurities such as metal and various forms of carbon.[16−20] Consequently, various purification methods have been applied in attempts to obtain carbon nanotubes with higher purity.[21−24] However, the purification methods give rise to structural and chemical changes in the SWNTs. Such changes are likely to alter the physical properties and adsorption behavior of SWNTs, and the relationship between the adsorption properties and such changes is worthy of study. Chiang et al.[25] investigated the purification and characterization of HiPco SWNT (HPNT) aggregates, but they did not report on the adsorption properties of HPNT aggregates.

In an earlier letter,[26] we reported on the pore structure change in HPNTs that was brought about by purification with dissolution (D) and gasification-dissolution (GD) methods. In this article, the effects of purification on the adsorption behavior for CH_3OH and C_2H_5OH molecules at 303 K are described.

Experimental Section

Our HPNTs were purchased from Carbon Nanotechnologies Inc. The HPNT purification was done by two methods. In the D method, the HPNTs were immersed in 35% HCl and stirred at room temperature for 48 h. The precipitates were filtrated and then washed with distilled water three times. After the sample was dried in air for 24 h at room temperature, it was heated in Ar at 523 K for 4 h. These processes were repeated two times. In the GD method, the HPNTs were heated in a 100 mL min^{-1} air flow at 623 K for 30 min and then purified by the D method. Pitch-based ACFs[27] (P5 and P20; AD′ALL Co. Ltd.) were also used so that we could compare their C_2H_5OH adsorption properties with those of the HPNT samples.

Transmission electron microscope (TEM) images were obtained with a Topcon EM-002B instrument at a 200 kV accelerating voltage. Thermogravimetric analysis (TGA) was done in an oxygen atmosphere (oxygen: 1%, argon: 99%). The TGA was carried out from room temperature to 1273 K with a heating rate of 5 K min^{-1}. X-ray photoelectron spectra (XPS) were obtained using an ESCA-850 (Shimadzu) instrument. The measurements were done with Mg Kα excitation in a vacuum ($<10^{-6}$ Pa) at room temperature. The acceleration tension and emission current of the nonmonochromatized X-ray source were 7 kV and 30 mA, respectively. The XPS spectra of all the samples were calibrated using the C1s peak of graphitic carbon at 284.6 eV.

[†] NEC Corporation.
[‡] Faculty of Science, Chiba University.
[§] Center for Frontier Electronics and Photonics, Chiba University.
[||] Meijo University.

10.1021/jp025767n CCC: $22.00
Published on Web 08/06/2002

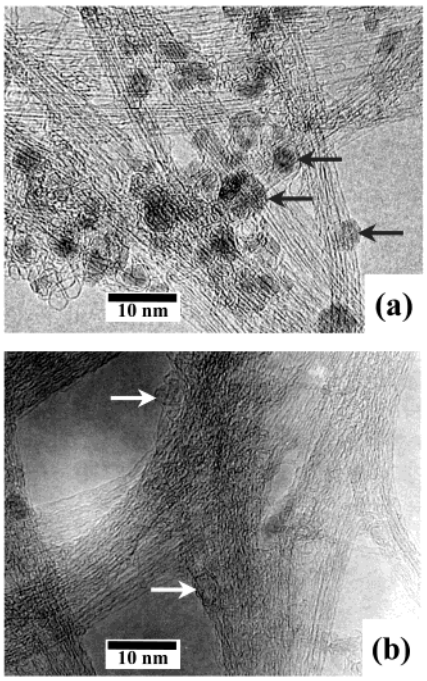

Figure 1. TEM images of pristine and purified HPNT aggregates: (a) pristine HPNTs; (b) GD-HPNTs.

The micropore structures were determined through the adsorption of N_2 at 77 K using volumetric equipment (Quantachrome AS-1-MP) after preevacuation for 2 h at 423 K and 10^{-4} Pa. The micropore structural parameters were obtained from high-resolution α_s plots constructed using the standard adsorption data for highly crystalline nonporous carbon black (Mitsubishi 4040B).[28]

The adsorption isotherms of CH_3OH and C_2H_5OH on the samples were gravimetrically measured at 303 K. The samples were preevacuated at 10^{-4} Pa and 423 K for 2 h. CH_3OH and C_2H_5OH were purified by means of a repeated freeze−pump−thaw cycle before being introduced into the adsorption cell. The irreversible adsorption amount of C_2H_5OH was determined from the amount of residual C_2H_5OH after the evacuation (10^{-3} Pa) at each temperature (303 K to 423 K) for 1 h.

Results and Discussion

Figure 1a shows a TEM image of an HPNT aggregate without any purification. Disordered carbon and spherical nanoparticles of Fe or Fe−C coated with graphene layers and with a diameter of several nanometers were observed in the pristine HPNT aggregates (as indicated by black arrows). Figure 1b shows a TEM image of a GD-HPNT aggregate. The purification treatment by the GD method remarkably decreased the nanoparticles of Fe or Fe−C, and thereby holes were produced in the HPNT aggregates (as indicated by white arrows). The TEM image of the GD-HPNT aggregate also showed the enhanced arrangement of HPNTs. Such a change in the assembly structure after purification was expected to create the micropores. However, since the TEM images cannot provide the quantitative information on the porosity change, detailed analysis of N_2 adsorption isotherms is necessary, as described below. The nanotube diameter would have ranged from 0.79 to 1.20 nm according to a Raman study on pristine HPNTs reported by Yudasaka et al.[29]

TGA was done to determine the oxidation stability and Fe content of the nanotube samples (Figure 2). The residual components after oxidation at 1173 K were expected to be iron oxides. The Fe content, determined by assuming that the iron oxides were composed of equal amounts of Fe_2O_3 and Fe_3O_4, fell from 27 to 18 and 6 wt % after purification by the D and GD methods, respectively. Purification by HCl-washing only provided limited removal of Fe from the nanotube aggregates because the Fe nanoparticles were coated with graphene sheets. The oxidation of the HPNTs shifted to a slightly higher temperature after purification by the D method. In contrast, the oxidation temperature of the GD-HPNTs increased markedly from 670 to 870 K. These results should be associated with the Fe content contained in the nanotube aggregates. It is well-known that many transition metals and their oxides play a catalytic role in the gasification of carbon materials. Consequently, a reduced Fe content after purification would result in a weaker catalytic effect on the reactivity of the nanotubes with regard to oxygen.

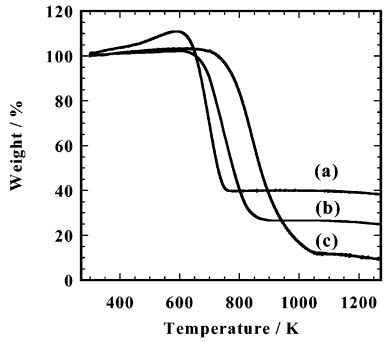

Figure 2. TGA curves of pristine and purified HPNTs: (a) pristine HPNTs; (b) D-HPNTs; (c) GD-HPNTs.

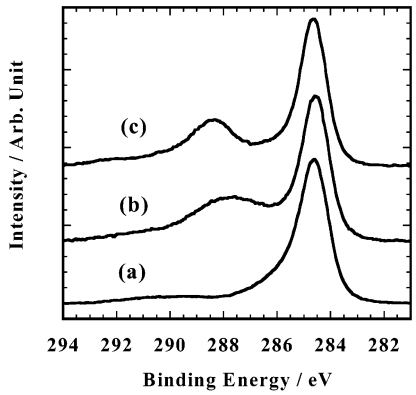

Figure 3. C1s XPS spectra of pristine and purified HPNTs: (a) pristine HPNTs; (b) D-HPNTs; (c) GD-HPNTs.

We used XPS to confirm the changes in the surface chemistry of the carbon nanotubes that resulted from the purification, since the surface chemistry is important to the adsorption phenomena. Figure 3 shows the XPS spectral change of the C1s peaks of pristine and purified HPNTs. The pristine HPNTs showed a peak of typical graphitic carbon at 284.6 eV. The purification treatments changed the C1s peak considerably at high binding energies. The D-HPNTs had a pronounced shoulder from 286 to 291 eV, which we assigned to the C−OH or C−O−C groups at 286.1 eV, the C=O group at 287.6 eV, and the COOH group at 288.6 eV.[30,31] The GD-HPNTs also had a pronounced shoulder at 287−291 eV, but it shifted to a binding energy higher than that of the D-HPNTs. These results provide evidence that oxygen-based functional groups were introduced to the nanotube surface after the purification treatments. Figure 4 shows the XPS spectral change in the O1s peaks of the pristine and purified HPNTs. The pristine HPNTs had two peaks, one

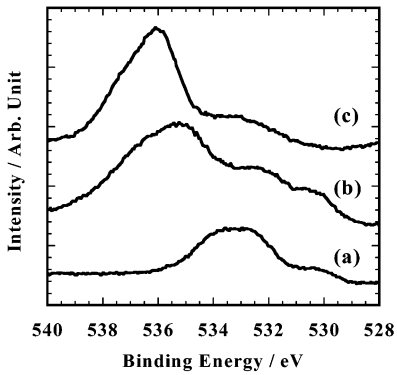

Figure 4. O1s XPS spectra of pristine and purified HPNTs: (a) pristine HPNTs; (b) D-HPNTs; (c) GD-HPNTs.

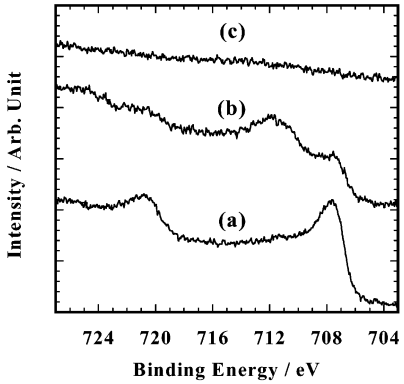

Figure 5. Fe2p XPS spectra of pristine and purified HPNTs: (a) pristine HPNTs; (b) D-HPNTs; (c) GD-HPNTs.

at 529−531 and one at 531−536 eV; these peaks can be respectively assigned to metal oxide[32] and C−OH or C−O−C.[33] In the case of the D-HPNTs, a new clear peak appeared at 534−538 eV, and this can be assigned to chemisorbed oxygen or water.[33] The O1s XPS spectra for the GD-HPNTs also show a peak at 534−538 eV, but the peak at 529−531 eV is barely visible. Figure 5 shows the XPS spectral change in the Fe2p peaks of the pristine and purified HPNTs. The pristine HPNTs had two peaks at binding energies of 720 and 707 eV, which were assigned to the metallic $Fe2p_{1/2}$ and $Fe2p_{3/2}$ peaks, respectively.[32,34−37] The Fe2p XPS spectra for the D-HPNTs show typical Fe2p peaks of Fe_2O_3 or Fe_3O_4 at 724 and 711 eV, as well as metallic Fe2p peaks.[32,34−37] These additional peaks were due to partial oxidation of the metallic Fe. On the other hand, the Fe2p XPS spectra for the GD-HPNTs had no peaks, although the Fe content determined from the TGA result was 6 wt %. These results suggest that XPS cannot detect the Fe from the GD-HPNT aggregates because the Fe nanoparticles are coated with graphene sheets.

We examined the pore structures of HPNT aggregates before and after purification treatments using the N_2 adsorption at 77 K. Figure 6 shows N_2 adsorption isotherms of HPNT samples at 77 K. The N_2 adsorption isotherm of the HPNTs is initially of type II and changes to type IV (having a hysteresis loop) as a result of both purification methods. The pore structure parameters of the samples, determined through the subtracting pore effect (SPE) method,[38] are summarized in Table 1. Purification by the D and GD methods increased the total surface area and micropore volume (which was accompanied by decreases in the external surface area and mesopore volume) and decreased the average pore width from 3.5 to 1.7 nm (D method) and 1.0 nm (GD method). These results probably reflect the formation of an oriented assembly structure due to the

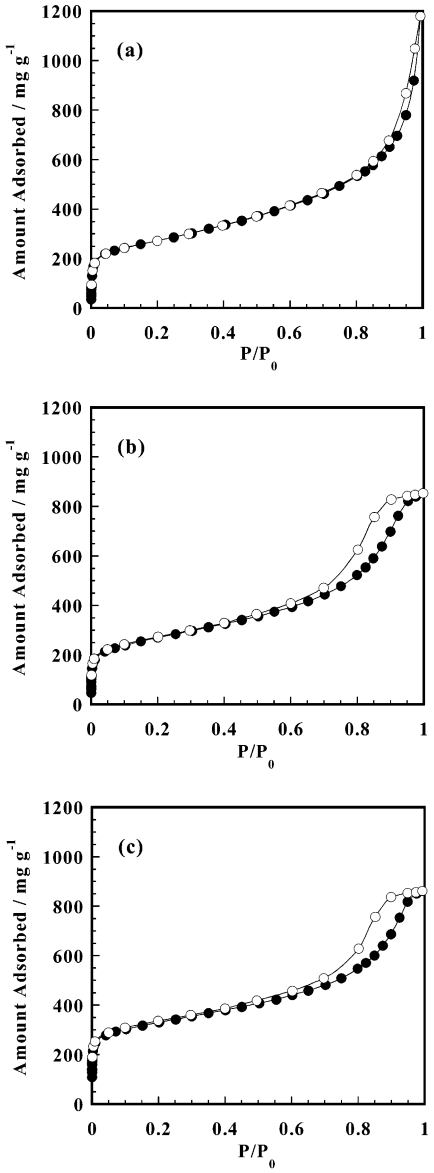

Figure 6. N_2 adsorption isotherms of pristine and purified HPNTs at 77 K: (a) pristine HPNTs; (b) D-HPNTs; (c) GD-HPNTs. The solid and open circles indicate adsorption and desorption branches, respectively.

TABLE 1: Pore Structure of HPNT and ACF Samples Determined by SPE Method

sample	tot. surf. area a_t (m^2 g^{-1})	ext surf. area a_{ext} (m^2 g^{-1})	micropore vol $W_0^{N_2}$ (mL g^{-1})	av pore width w (nm)
HPNT	524	436	0.15	3.5
D-HPNT	587	364	0.19	1.7
GD-HPNT	861	334	0.27	1.0
P5	790	10	0.26	0.7
P20	1430	25	0.79	1.1

removal of Fe impurities. A detailed explanation concerning the pore structures of HPNT samples before and after purification was given in our earlier article.[26]

Figure 7 shows the adsorption isotherms of C_2H_5OH for pristine and purified HPNTs at 303 K. All C_2H_5OH adsorption isotherms were close to type II, although they had a small hysteresis loop. The hysteresis loops became slightly larger after the purification treatments. The purification treatments also enhanced the amount of C_2H_5OH adsorption until $P/P_0 = 0.9$, which we associate mainly with the enhanced porosity. Figure 8 shows the C_2H_5OH adsorption isotherms with a logarithmic-

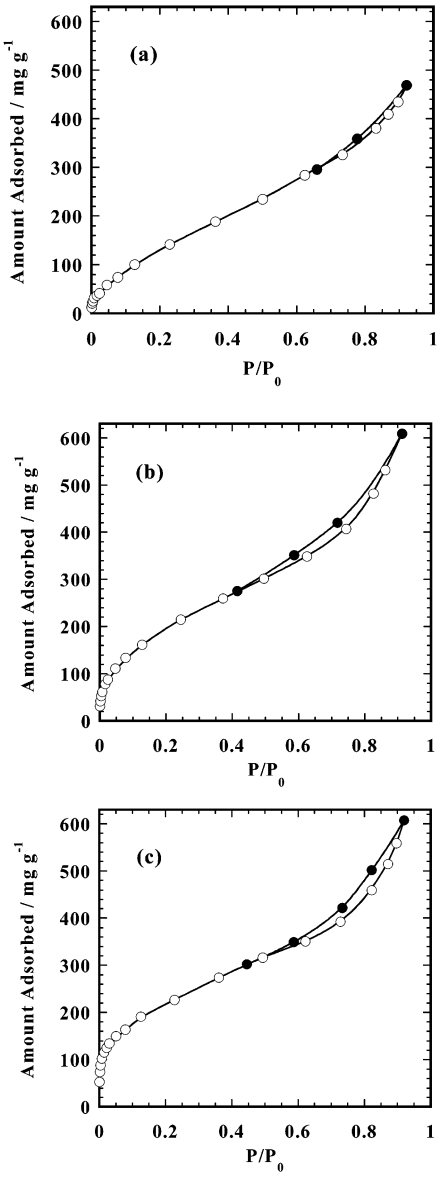

Figure 7. C_2H_5OH adsorption isotherms on pristine and purified HPNTs at 303 K: (a) pristine HPNTs; (b) D-HPNTs; (c) GD-HPNTs. The open and solid circles indicate adsorption and desorption branches, respectively.

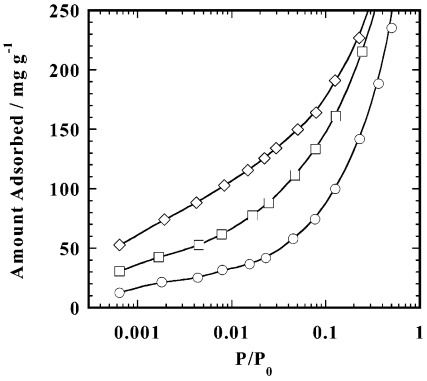

Figure 8. C_2H_5OH adsorption isotherms in logarithmic scale on pristine and purified HPNTs at 303 K: (○) pristine HPNTs; (□) D-HPNTs; (◇) GD-HPNTs.

scale abscissa to allow comparison of the C_2H_5OH adsorption behavior at low pressure. The GD-HPNTs showed a remarkably enhanced adsorption amount (to about 53 mg g^{-1}) of C_2H_5OH below $P/P_0 = 0.001$. The C_2H_5OH adsorption amount at $P/P_0 = 0.000\,64$ on the D-HPNTs also increased from 13 to 31 mg g^{-1}. The adsorption behavior of polar molecules on porous carbon at low pressure should be associated not only with the dispersion interaction in micropores but also with the polarity of the adsorbent surface. Figure 9a compares the C_2H_5OH adsorption isotherms for HPNT samples with those for ACF samples (using a logarithmic scale). P20 has a very high surface area and micropore volume.[27] The average pore width of P20 is close to that of the GD-HPNTs (Table 1). Although the GD-HPNT micropore volume was about one-third that of P20, a much larger amount of C_2H_5OH was adsorbed on the GD-HPNTs below $P/P_0 = 0.01$ than on P20, indicating the strong interaction of the C_2H_5OH molecules with the GD-HPNT surface. P5 has a small average pore width of 0.7 nm, and the P5 micropore volume is similar to that of GD-HPNTs.[27] However, P5 with its small pore width also showed less adsorption than the purified HPNTs at low relative pressure. Figure 9b also compares the C_2H_5OH adsorption isotherms for HPNT samples with those for ACF samples, but here the ordinate is expressed in the weight of adsorbed C_2H_5OH per unit pore volume, determined from α_s plots of the N_2 adsorption isotherms at 77 K. In this case, the GD-HPNTs showed a large adsorption amount of about 200 mg mL^{-1}. In addition, the difference in the amounts of adsorbed C_2H_5OH between the GD-HPNT and the ACF samples became larger. Such strong interaction is likely to have been caused by the increment of hydrogen bonding sites by oxygen-based functional groups. These results suggest that C_2H_5OH adsorption at very low relative pressure should predominantly depend on the polarity of the pore-wall surface.

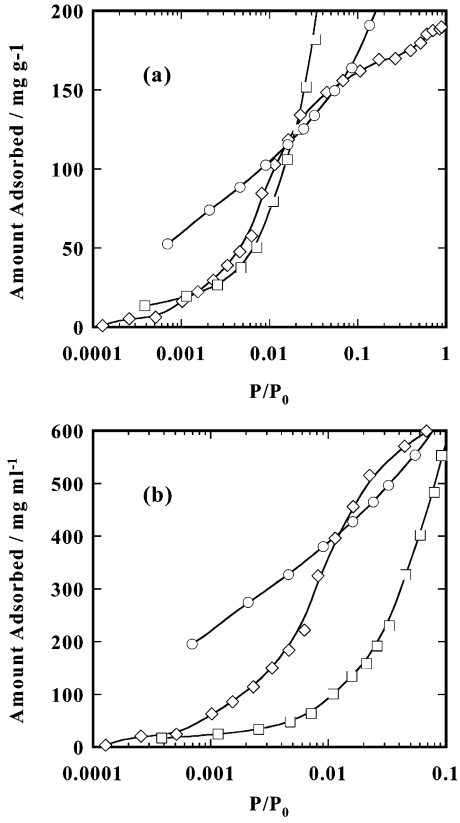

Figure 9. Comparison of C_2H_5OH adsorption isotherms of GD-HPNTs with ACF samples in logarithmic scale: (a) adsorbed amount; (b) adsorbed amount relative to the micropore volume [(○) GD-HPNTs; (□) P20; (◇) P5].

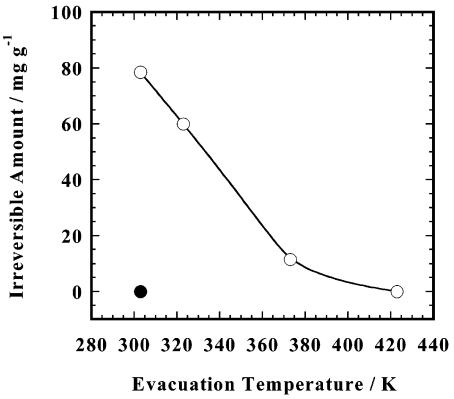

Figure 10. Evacuation temperature dependence of the irreversible amount of C_2H_5OH adsorbed on HPNT samples: (●) pristine HPNTs; (○) GD-HPNTs.

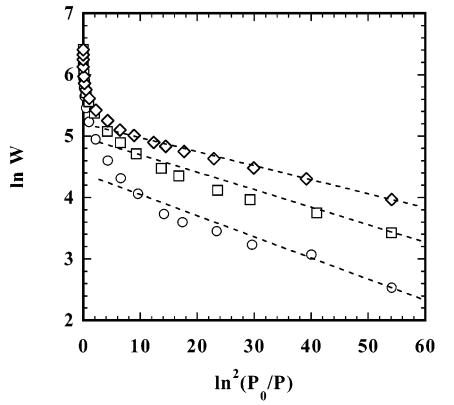

Figure 11. DR plots of C_2H_5OH adsorption isotherms on HPNT samples: (○) pristine HPNTs; (□) D-HPNTs; (◇) GD-HPNTs.

Figure 10 shows the evacuation temperature dependence of the irreversible amount of C_2H_5OH adsorbed on the GD-HPNTs. For pristine HPNTs, the amount of residual C_2H_5OH molecules was almost zero after evacuation at 303 K and 10^{-3} Pa for 1 h. On the other hand, the GD-HPNTs had an irreversible amount of about 78 mg g^{-1} after evacuation under the same conditions. Even evacuation at 373 K could not completely remove the adsorbed C_2H_5OH molecules. These results reflect a very strong interaction between adsorbed C_2H_5OH molecules and oxygen-based functional groups on the nanotube surface. We can consider this phenomenon from a different standpoint. It is well-known that a carboxylic acid is converted into an ester by heating in the presence of an alcohol and a small amount of dry HCl. Therefore, it is possible that the COOH group introduced on the nanotube surface, as was confirmed by XPS, is converted into an ester by the adsorbed C_2H_5OH and the HCl that remained after the HCl-washing.

Figure 11 shows Dubinin−Radushkevich (DR) plots for the C_2H_5OH adsorption isotherms on the nanotube samples. All the DR-plots were linear in the low-pressure range. The micropore volume W_0^{EtOH} and $q_{st,\phi=1/e}$ determined from these DR plots are shown in Table 2. Micropore volumes from the DR equation are given by

$$\ln W = \ln W_0 - (A/\beta E_0)^2$$
$$A = RT \ln (P_0/P) \qquad (1)$$

where W is the amount of adsorption for P/P_0 and W_0 is the micropore volume, A is the adsorption potential, β is the affinity coefficient, and E_0 is the characteristic adsorption energy. Furthermore, βE_0 gives the isosteric heat of adsorption at a fractional filling ϕ of e^{-1},

$$\beta E_0 + \Delta H_v = q_{st,\phi=1/e} \qquad (2)$$

Here, ΔH_v is the enthalpy of vaporization. We used a liquid density of 0.7868 g mL^{-1}, β of 0.65, and ΔH_v of 38.6 kJ mol^{-1} for C_2H_5OH in this analysis. The values of $q_{st,\phi=1/e}$ increased as a result of purification. The heat of adsorption depended on the pore width and the pore-wall chemistry. That is, the greater $q_{st,\phi=1/e}$ values indicated a stronger adsorbate−pore interaction. The $q_{st,\phi=1/e}$ value for the GD-HPNTs showed a meaningful increase of 2.1 kJ mol^{-1} compared to that for the HPNTs. The $q_{st,\phi=1/e}$ value for the D-HPNTs was also larger than that for the HPNTs. We attributed these results to the developed microporosity and the polar functional groups introduced on the surface. W_0^{EtOH} values also increased after the purification treatments. The ratio of W_0^{EtOH} to $W_0^{N_2}$, which indicates the accessibility of C_2H_5OH molecules to the micropores, was 0.53, 0.79, and 0.82, respectively, for the HPNTs, D-HPNTs, and GD-HPNTs (Table 2). Better accessibility for the C_2H_5OH molecules is likely to be realized when the molecules become orientated with each other within the restricted space, and purification treatments greatly enhance the orientation of adsorbed C_2H_5OH molecules. These results suggest that the polar functional groups introduced by purification treatments acutely affect the ordered structure of adsorbed C_2H_5OH molecules.

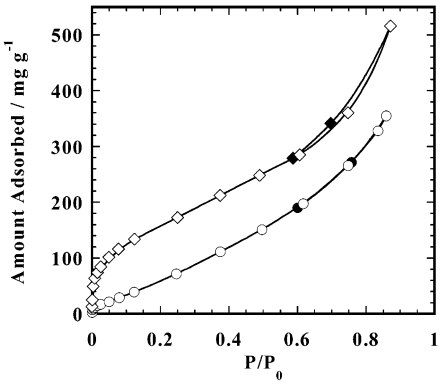

Figure 12. CH_3OH adsorption isotherms on pristine HPNTs and GD-HPNTs at 303 K: (○) pristine HPNTs; (◇) GD-HPNTs. The open and solid symbols respectively indicate adsorption and desorption branches.

TABLE 2: Micropore Volume W_0^{EtOH} and Isosteric Heat of Adsorption $q_{st,\phi=1/e}$ Determined from DR Plots of C_2H_5OH Adsorption Isotherms at 303 K

sample	W_0^{EtOH} (mL g^{-1})	$q_{st,\phi=1/e}$ (kJ mol^{-1})	$W_0^{EtOH}/W_0^{N_2}$
HPNT	0.08	53.5	0.53
D-HPNT	0.15	54.5	0.79
GD-HPNT	0.22	55.6	0.82

Figure 12 shows the adsorption isotherms of CH_3OH on pristine HPNTs and GD-HPNTs at 303 K. Both CH_3OH adsorption isotherms are close to type II. However, the HPNT isotherm shows very little adsorption uptake at low relative pressure, indicating a weak interaction between the carbon nanotube surface and CH_3OH molecules. However, the purification treatment greatly increased the CH_3OH adsorption capacity, as was the case with the C_2H_5OH adsorption.

Parts a and b of Figure 13 show the adsorption isotherms of CH_3OH and C_2H_5OH on pristine HPNTs and GD-HPNTs, respectively. Here the ordinate is expressed as the number of

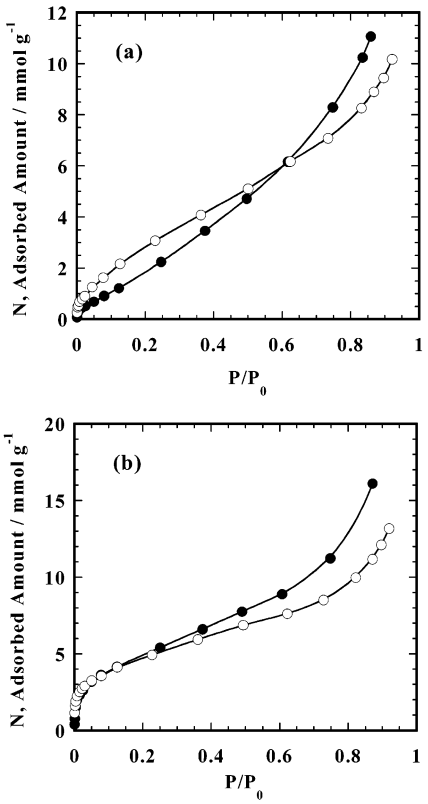

Figure 13. CH_3OH and C_2H_5OH adsorption isotherms on HPNT samples at 303 K: (a) pristine HPNTs; (b) GD-HPNTs: (●) CH_3OH; (○) C_2H_5OH.

moles of adsorbed molecules per unit weight (N). For the pristine HPNTs, N of C_2H_5OH was larger than that of CH_3OH at low relative pressure, which we associate with the weaker dispersion interaction of CH_3OH with the carbon nanotube surface, which in turn reflects the low polarity. However, at higher relative pressure, N of C_2H_5OH was smaller than that of CH_3OH, which probably stemmed from the better packing of CH_3OH in the pores because of its smaller molecular size. Larger alcohol molecules can interact with the pores more strongly in the low-pressure region than smaller alcohol molecules, and thereby a perfect packing structure formation is more difficult to achieve with larger alcohol molecules in the micropores than with small alcohol molecules.[39] The similar result that we observed can be explained in the same way. Ohkubo and Kaneko[40] showed the relationship between the adsorbed density and the orientation of alcohol molecules by applying an in situ X-ray diffraction technique. However, for GD-HPNTs there is almost no difference between the N values for C_2H_5OH and CH_3OH at $P/P_0 < 0.2$. In addition, a reversal of their N values was observed at the lower relative pressure. This result suggests that the adsorption interaction between CH_3OH molecules and the GD-HPNT pore wall is enhanced by the increased number of hydrogen bonding sites after purification.

These results regarding alcohol adsorption clearly show that the chemical purification affects the mutually aggregated structure of SWNTs as well as their surface chemistry. It is well-known that chemical treatment can change the surface chemistry of porous materials, but the change in the surface oxygen content caused by purification has not been closely examined. The higher-order structural change caused by chemical purification should be stressed, however, since the higher-order structure of SWNTs determines both the microporosity and the mesoporosity, which govern the adsorption properties.

Acknowledgment. We thank the Japan Science and Technology Corporation for supporting this International Cooperative Research Project.

References and Notes

(1) Iijima, S. *Nature* **1991**, *354*, 56.
(2) Iijima, S.; Ichihashi, T. *Nature* **1993**, *363*, 603.
(3) Dillon, A. C.; Jones, K. M.; Bekkedahl, T. A.; Kiang, C. H.; Bethune, D. S.; Heben, M. S. *Nature* **1997**, *386*, 377.
(4) Liu, C.; Fan, Y. Y.; Liu, M.; Cong, H. T.; Cheng, H. M.; Dresselhaus, M. S. *Science* **1999**, *286*, 1127.
(5) Ye, Y.; Ahn, C. C.; Witham, C.; Fultz, B.; Liu, J.; Rinzler, A. G.; Colbert, D. T.; Smith, K. A.; Smalley, R. E. *Appl. Phys. Lett.* **1999**, *74*, 2307.
(6) Rinzler, A. G.; Hafner, J. H.; Nikolaev, P.; Lou, L.; Kim, S. G.; Tomanek, D.; Nordlander, P.; Colbert, D. T.; Smalley, R. E. *Science* **1995**, *269*, 1550.
(7) Niu, C.; Sichel, E. K.; Hoch, R.; Moy, D.; Tennent, H. *Appl. Phys. Lett.* **1997**, *70*, 1480.
(8) An, K. H.; Kim, W. S.; Park, Y. S.: Lim, I. S.; Bae, D. J.; Lee, S. M.; Choi, Y. C.; Lee, Y. H. *Adv. Mater.* **2001**, *13*, 497.
(9) Tanaka, H.; El-Merraoui, M.; Steele, W. A.; Kaneko, K. *Chem. Phys. Lett.* **2002**, *352*, 334.
(10) Kaneko, Y.; Ohbu, K.; Uekawa, N.; Fujie, K.; Kaneko, K. *Langmuir* **1995**, *11*, 708.
(11) Rodriguez-Reinoso, F.; Molina-Sabio, M.; Munecas M. A. *J. Phys. Chem.* **1992**, *96*, 2707.
(12) Lee, W. H.; Reucroft, P. J. *Carbon* **1999**, *37*, 7.
(13) Mangun, C. L.; Benak, K. R.; Daley, M. A.; Economy, *J. Chem. Mater.* **1999**, *11*, 3476.
(14) Yang, C. M.; Kaneko, K. *Carbon* **2001**, *39*, 1075.
(15) Yang, C. M.; Kaneko, K. *J. Colloid Interface Sci.* **2002**, *246*, 34.
(16) Shi, Z. J.; Lian, Y. F.; Liao, F. H.; Zhou, X. H.; Gu, Z. N.; Zhang, Y.; Iijima, S. *Solid State Commun.* **1999**, *112*, 35.
(17) Journet, C.; Maser, W. K.; Bernier, P.; Loiseau, A.; de la Chapelle, M. L.; Lefrant, S.; Deniard, P.; Lee, R.; Fischer, J. E. *Nature* **1997**, *388*, 756.
(18) Kong, J.; Cassell, A. M.; Dai, H. *Chem. Phys. Lett.* **1998**, *292*, 567.
(19) Cassell, A. M.; Raymakers, J. A.; Kong, J.; Dai, H. *J. Phys. Chem. B* **1999**, *103*, 6484.
(20) Nikolaev, P.; Bronikowski, M. J.; Bradley, R. K.; Rohmund, F.; Colbert, D. T.; Smith, K. A.; Smalley, R. E. *Chem. Phys. Lett.* **1999**, *313*, 91.
(21) Shelimov, K. B.; Esenaliev, R. O.; Rinzler, A. G.; Huffman, C. B.; Smalley, R. E. *Chem. Phys. Lett.* **1998**, *282*, 429.
(22) Zimmerman, J. L.; Bradley, R. K.; Huffman, C. B.; Hauge, R. H.; Margrave, J. L. *Chem. Mater.* **2000**, *12*, 1361.
(23) Moon, J. M.; An, K. H.; Lee, Y. H.; Park, Y. S.; Bae, D. J.; Park, G. S. *J. Phys. Chem. B* **2001**, *105*, 5677.
(24) Chiang, I. W.; Brinson, B. E.; Smalley, R. E.; Margrave, J. L.; Hauge, R. H. *J. Phys. Chem. B* **2001**, *105*, 1157.
(25) Chiang, I. W.; Brinson, B. E.; Huang, A. Y.; Willis, P. A.; Bronikowski, M. J.; Margrave, J. L.; Smalley, R. E.; Hauge, R. H. *J. Phys. Chem. B* **2001**, *105*, 8297.
(26) Yang, C. M.; Kaneko, K.; Yudasaka, M.; Iijima, S. *Nano Lett.* **2002**, *2*, 385.
(27) Ohkubo, T.; Iiyama, T.; Nishikawa, K.; Suzuki, T.; Kaneko, K. *J. Phys. Chem. B* **1999**, *103*, 1859.
(28) Murata, K.; Kaneko, K.; Kokai, F.; Takahashi, K.; Yudasaka, M.; Iijima, S. *Chem. Phys. Lett.* **2000**, *331*, 14.
(29) Yudasaka, M.; Kataura, H.; Ichihashi, T.; Qin, L. C.; Kar, S.; Iijima, S. *Nano Lett.* **2001**, *1*, 487.
(30) Gardner, S. D.; Singamsetty, C. S. K.; Booth, G. L.; He. G. R. *Carbon* **1995**, *33*, 587.
(31) Yue, Z. R.; Jiang, W.; Wang, L.; Gardner, S. D.; Jr. Pittman, C. U, *Carbon* **1999**, *37*, 1785.
(32) Moore, R. G. C.; Evans, S. D.; Shen, T.; Hodson, C. E. C. *Physica E* **2001**, *9*, 253.
(33) Biniak, S.; Szymanski, G.; Siedlewski, J.; Swiatkowski, A. *Carbon* **1997**, *35*, 1799.
(34) Graat, P. C. J.; Somers, M. A. J. *Appl. Surf. Sci.* **1996**, *36*, 100.
(35) Roosendaal, S. J.; Asselen, B. V.; Elsenaar, J. W.; Vredenberg, A. M.; Habraken, F. H. P. M. *Surf. Sci.* **1999**, *442*, 329.
(36) Voss, M.; Borgmann, D.; Wedler, G. *Surf. Sci.* **1999**, *433−435*, 559.
(37) Kim, K. J.; Moon, D. W.; Lee. S. K.; Jung, K. H. *Thin Solid Films* **2000**, *360*, 118.
(38) Setoyama, N.; Suzuki, T.; Kaneko, K. *Carbon* **1998**, *36*, 1459.
(39) Bradley, R. H.; Rand, B. *Carbon* **1991**, *29*, 1165.
(40) Ohkubo, T.; Kaneko, K. *Colloid Surf.* **2001**, *187−188*, 177.